

Weak-Field Magnetoresistance and the Valence-Band Structure of SnTe[†]

R. S. Allgaier and Bland Houston

Naval Ordnance Laboratory, Silver Spring, Maryland 20910

(Received 9 September 1971)

Weak-field magnetoresistance measurements on *p*-type SnTe exhibit a peculiar symmetry which is temperature and carrier-concentration dependent. A Fermi-surface model is described which can account for these results and reconcile them with several other kinds of experimental measurements on SnTe. The Fermi surface consists of four prolate $\langle 111 \rangle$ valleys with three $\langle 100 \rangle$ -oriented knobs protruding from each end of each valley. The proposed model is also used to bring out some previously unreported similarities between the band structures of the $\text{Pb}_{1-x}\text{Sn}_x\text{Te}$ and $\text{Bi}_{1-x}\text{Sb}_x$ systems, and to examine the broader question of the connection between weak-field magnetoresistance behavior and band-structure characteristics.

I. INTRODUCTION

Some time ago, we found that the weak-field magnetoresistance in *p*-type SnTe exhibits a peculiar symmetry which, moreover, is a strong function of both carrier density and temperature.^{1,2} The main purpose of this paper is to describe a conceptually simple model which can account for this unusual behavior in a straightforward way.³

Section II is concerned with experimental details, and Sec. III presents and discusses the magnetoresistance (MR) measurements. Because of their unusual nature, the question of the reliability of the data is examined in some detail. The apparently contradictory nature of the weak-field MR and strong-field data is next considered, and two earlier attempts to explain the weak-field MR are briefly reexamined.

A new model is then proposed, and its relevance to the weak-field MR data, as well as to the elastic constants and the elastoresistance of SnTe, is examined. Some observations about the qualitative behavior of the thermoelectric power, Hall coefficient, and Hall mobility are also included. The final section of the discussion considers some of the unifying features of the band structures of the $\text{Pb}_{1-x}\text{Sn}_x\text{Te}$ and $\text{Bi}_{1-x}\text{Sb}_x$ systems.

The column-V semimetals (As, Sb, Bi) and the IV-VI semiconducting compounds (IV = Ge, Sn, or Pb; VI = S, Se, or Te) form a close-knit family of materials with a number of similar physical and electronic properties. These similarities are discussed in many of the papers from three conferences which dealt with the materials.⁴⁻⁶

Both PbTe and SnTe crystallize in the NaCl structure, and form single-phase alloys at all compositions. Excess Pb and Te make PbTe *n* and *p* type, respectively, but in the case of SnTe, the solidus field lies entirely on the Te-rich side of stoichiometry. Many different properties of the two compounds have been studied extensively. Here we

will only mention four relevant types of measurements—electrical, galvanomagnetic, thermoelectric transport, and optical—on⁷⁻³¹ PbTe and SnTe.^{1,2,13,25,32-57}

Information has been derived from these measurements concerning the temperature, carrier-concentration, and directional dependences of the effective masses in the conduction and valence bands of the two materials. This in turn has led to the development of a basic band-structure model with some distinctive features which, in general, are in agreement with a series of theoretical calculations.⁵⁸⁻⁷⁴

Almost all of the experimental and theoretical studies on PbTe and SnTe just cited suggest that the electronic properties of the two compounds are qualitatively the same in the following respects:

(i) The main conduction- and valence-band edges occur at or near the centers of the hexagonal faces (the *L* points) of the fcc Brillouin zone. In the case of PbTe, this location was originally suggested by weak-field MR measurements.^{7,8,10,11}

(ii) The constant-energy surfaces near the main valence-band maxima have a highly prolate $\langle 111 \rangle$ -oriented form. The most direct evidence for this comes from the Shubnikov-de Haas and de Haas-van Alphen measurements.^{15,29,31,39,43,54}

(iii) A significantly nonparabolic energy-momentum relationship occurs over most, if not all, of the carrier densities thus far studied (the range is, roughly, 10^{17} – 10^{21} cm⁻³).

(iv) A set of subsidiary maxima in the valence band also plays an important role in the conduction process in *p*-type samples. These maxima most probably lie along the $\langle 110 \rangle$ axes (the Σ axes) of the Brillouin zone, roughly halfway between the zone center and zone boundaries. Henceforth, the conduction-band minima will be identified as CB(*L*) and the main and subsidiary maxima of the valence band as VB(*L*) and VB(Σ), respectively.

It has become traditional to refer to the subsid-

ary maxima as a “second valence band,”⁷⁵ but the band calculations have made it quite clear that *both sets of maxima belong to the same valence band*. The importance of this distinction will become evident later.

(v) In *p*-type samples above about 150 K, significant numbers of holes begin to be thermally generated in the valence-band region near $VB(\Sigma)$. This was originally inferred from the temperature dependence of the Hall coefficient^{12,19,32} and from the energy dependence of the optical absorption.¹⁶ At lower temperatures, holes appear near $VB(\Sigma)$ only when the total density of positive carriers exceeds $1-2 \times 10^{20} \text{ cm}^{-3}$. This was deduced from the observation of kinks in the high-temperature-low-temperature Hall-coefficient ratio and in the thermoelectric power as functions of carrier density.^{27,28,33-36,38,40,47}

Many of the same types of measurements cited above for PbTe and SnTe have also been carried out on the alloy system $Pb_{1-x}Sn_xTe$.^{25,76-87} Some of the alloy data, as well as certain results on SnTe,^{42,44,45,52} led Dimmock, Melngailis, and Strauss to conclude, despite the similarities enumerated above, that there is an important difference between PbTe and SnTe.⁷⁸

This difference is illustrated in Fig. 1, which sketches the relative energies of the $CB(L)$, $VB(L)$, and $VB(\Sigma)$ extrema as functions of T (temperature) and x (composition, in $Pb_{1-x}Sn_xTe$). The composition dependence enters via an adjustable temperature scale. The figure shows that in PbTe the direct energy gap E_g between $CB(L)$ and $VB(L)$ decreases as T decreases or as SnTe is added to PbTe. Over a range of intermediate values of x , the two levels which determine E_g cross and interchange their roles at some T between 0 and 300 K.⁷⁹ For SnTe, the temperature coefficient of E_g is negative, opposite to that in PbTe, but similar to that found in most semiconductors.

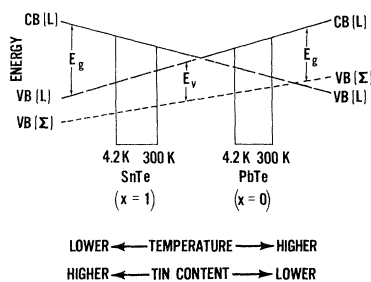


FIG. 1. Conduction- and valence-band extrema vs temperature in the $Pb_{1-x}Sn_xTe$ system. $CB(L)$ and $VB(L)$ denote the conduction-band minima and the valence-band maxima at the L points of the Brillouin zone. $VB(\Sigma)$ identifies a subsidiary set of maxima in the *same* valence band, located along the Σ (i. e., the $\langle 110 \rangle$) axes of the zone.

On the basis of Fig. 1, it might seem reasonable to expect that basic properties of the $Pb_{1-x}Sn_xTe$ system which depend strongly on the magnitude of E_g would exhibit a symmetrical behavior on opposite sides of the band-crossover point, but with a reversed temperature dependence. This anticipation, in general, is *not* borne out by the experimental data. The electric-susceptibility effective mass in *p*-type SnTe, for example, increases with increasing T at all carrier densities studied ($3.6 \times 10^{19} \leq p \leq 1.2 \times 10^{21} \text{ cm}^{-3}$).⁵⁷ In other words, its behavior resembles that found in PbTe where the positive mass-temperature coefficient has been explained in terms of the positive dE_g/dT found in that compound.^{14,17,18}

Another surprising result is the temperature dependence of the carrier mobility. It is essentially identical between 4.2 and 300 K in PbTe and SnTe samples with positive carrier densities of about $1 \times 10^{20} \text{ cm}^{-3}$.¹³ Furthermore, analyses which fitted a “two-valence-band” model to transport data on *p*-type SnTe as a function of temperature evidently found it necessary to assume a PbTe-like variation of the energy difference E_v (see Fig. 1) between the $VB(L)$ and $VB(\Sigma)$ maxima.^{25,40,46,47}

An explanation for these seemingly inconsistent results was proposed by the first author and by Burke and Riedl who used it to account for the unusual temperature-dependent shape of the optical-absorption edge in SnTe.⁵³ The explanation points out that the $CB(L)$ and $VB(L)$ energy levels shown in Fig. 1 refer only to one *point* in the Brillouin zone. It is also necessary to examine the temperature dependences of states in the conduction and valence bands from the *volume* of the zone within which carriers contribute to the property being analyzed.

This more complicated situation may be visualized as follows: As the temperature of a suitably chosen $Pb_{1-x}Sn_xTe$ alloy drops below the point at which the $CB(L)$ and $VB(L)$ extrema cross, a growing volume may be defined, inside of which the direct gap between the two bands has begun to increase with decreasing T . But outside of this volume, the gap is still decreasing with decreasing T , in PbTe-like fashion. Carriers from the latter region are evidently the dominant influence on the experimental results cited for *p*-type SnTe.

In view of the above remarks, it might well be anticipated that the form of the Fermi surfaces in the $Pb_{1-x}Sn_xTe$ system will evolve in a rather complicated fashion as x changes from 0 to 1. In fact, a number of the measurements of conductivity, Hall coefficient, and thermoelectric power do suggest that something out of the ordinary is taking place as a function of x .^{76,77,81,83,85}

Unfortunately, the Shubnikov-de Haas and de Haas-van Alphen effects are insensitive to the kind of Fermi-surface distortion proposed in Sec. III D.

Some complications have been observed in these effects in the alloys^{82,86} (but not always⁸⁴) and in SnTe,^{43,45} but they have been tentatively ascribed to growth striations and to a low-temperature phase change, respectively.

It now seems clear that the first strong experimental evidence that highly distorted Fermi surfaces appear in the $\text{Pb}_{1-x}\text{Sn}_x\text{Te}$ system was the weak-field MR data in p -type SnTe. It is the goal of this paper to demonstrate that the nature of those distortions can be inferred from the weak-field results.

On the theoretical side, some of the more recent SnTe band calculations^{67-69,72-74} also suggest that distorted Fermi surfaces should appear near the L points.

II. EXPERIMENTAL DETAILS

All measurements were carried out on oriented bulk samples of SnTe cut from large single crystals grown by the Czochralski method.⁸⁸ The nominal carrier density p^* of the as-grown crystals was about $8 \times 10^{20} \text{ cm}^{-3}$. Nominal carrier density is defined by the relation

$$p^* = 1/(R_0 |e|) \text{ cm}^{-3}, \quad (1)$$

where R_0 is the weak-field Hall coefficient in cm^3/C [measured in the low-temperature range (77 K or lower) where it does not vary with temperature] and e is the electronic charge in C.

Carrier densities higher or lower than the as-grown value were obtained using Brebrick's technique,³⁴ i. e., by annealing the samples at various temperatures in the presence of ingots containing large excesses of Te or Sn, respectively. In this way, the composition limits of stability at the particular annealing temperature can be reached after a sufficient time interval. In some cases, carrier densities on the boundaries of the solidus field and within it were obtained by vacuum-annealing samples which had been coated with relatively small amounts of Sn.³⁷

The sample dimensions were approximately $\frac{3}{4} \times 1 \times 5$ mm. Rhodium plates under spring pressure formed the current contacts, and rhodium spring wires with sharpened tips were used for the resistivity and Hall probes. Conventional dc measurements were made with a Rubicon microvolt potentiometer and a Guideline galvanometer. At a sample current of 400 mA and a magnetic field intensity of 10 kOe, the Hall and MR signals were in the 10^{-6} - and 10^{-7} -V ranges, respectively, and, as expected in weak magnetic fields, were proportional to the first and second powers of the field.

The MR at 295 and 77 K was measured with the sample directly immersed in water and in liquid nitrogen. Under these conditions, the Peltier heating and cooling at the sample ends produced a thermoelectric voltage across the resistivity probes

which was less than 1% of the total signal.

III. RESULTS AND DISCUSSION

A. Summary of Magnetoresistance Data

The most extensive MR measurements were obtained on [110]-oriented crystals with $p^* = 9 \times 10^{19}$ and $1.5 \times 10^{20} \text{ cm}^{-3}$. The Hall mobilities and three different MR coefficients at 295 and 77 K for these samples are summarized in Table I. Included for comparison are the same quantities published earlier on PbTe at $p^* = 3 \times 10^{18} \text{ cm}^{-3}$.¹¹

The MR data shown in the table are the dimensionless coefficients $M_{\alpha\beta\gamma}^{\delta\epsilon\zeta}$ defined by

$$\Delta\rho/\rho_0 = M_{\alpha\beta\gamma}^{\delta\epsilon\zeta} (\mu_H H/C)^2, \quad (2)$$

where $\Delta\rho/\rho_0$ is the fractional change in the zero-field resistivity, $\alpha\beta\gamma$ and $\delta\epsilon\zeta$ identify the sample-current and magnetic field directions with respect to the cubic axes of the crystal, $\mu_H (= R/\rho_0)$ is the Hall mobility, H is the magnetic field intensity, and C is the "compatibility factor" which equals 10^8 (no dimensions) when μ_H is in $\text{cm}^2/\text{V sec}$ and H is in Oe.

Following these data in Table I are the dimensionless Seitz coefficients b , c , and d . They are determined from the experimental $M_{\alpha\beta\gamma}^{\delta\epsilon\zeta}$ values by using the relationship

$$M_{\alpha\beta\gamma}^{\delta\epsilon\zeta} = b + c (\sum_j \iota_j \eta_j)^2 + d (\sum_j \iota_j^2 \eta_j^2), \quad (3)$$

where ι_j and η_j are the direction cosines of the sample-current and magnetic field directions relative to the cubic axes of the crystal.

The final line of Table I presents values of the MR symmetry parameter z , defined as

$$z = -(b+c)/d, \quad (4)$$

and determined from the experimental data. It is the behavior of this symmetry parameter which leads us to describe the SnTe weak-field MR data as "peculiar."

Some incomplete sets of MR measurements (i. e., insufficient to determine b , c , and d) were obtained at lower and higher carrier densities. For reasons to be discussed in Sec. III B, we regard them as less reliable than those presented in Table I.

However, one of these incomplete measurements will be mentioned because it seems quite relevant to the model which will be proposed in Sec. III D. Room-temperature MR data on a [110]-oriented as-grown crystal ($p^* \approx 8 \times 10^{20} \text{ cm}^{-3}$) led to the result $M_{110}^{001} = M_{110}^{110} = 2.3$. According to Eq. (3), this equality requires that $d=0$.

B. Reliability of Data

Because the MR data are so peculiar, it is essential to examine carefully the question of their reliability.

TABLE I. Experimental weak-field magnetoresistance, Hall mobilities, Seitz magnetoresistance coefficients, and magnetoresistance symmetry parameters for p -type PbTe and SnTe crystals.

Compound	PbTe		SnTe		SnTe	
	3×10^{18}		9×10^{18}		1.5×10^{20}	
Nominal carrier density ^a (cm ⁻³)						
Temperature (K)	295	77	295	77	295	77
Hall mobility (cm ² /V sec)	888	15 500	823	2510	510	1330
M_{110}^{110} ^b	0.275	0.196	0.46 ± 0.03^c	0.57 ± 0.03^c	0.69 ± 0.03^c	1.00 ± 0.03^c
M_{110}^{001} ^b	0.345	0.151	0.56 ± 0.03	0.58 ± 0.03	0.86 ± 0.03	1.13 ± 0.03
$M_{110}^{1\bar{1}0}$ ^b	0.605	0.348	0.72 ± 0.03	0.66 ± 0.03	1.04 ± 0.03	1.20 ± 0.03
b^d	0.345	0.151	0.56 ± 0.03	0.58 ± 0.03	0.86 ± 0.03	1.13 ± 0.03
c^d	-0.330	-0.152	-0.26 ± 0.04	-0.09 ± 0.04	-0.35 ± 0.04	-0.20 ± 0.04
d^d	0.520	0.394	0.32 ± 0.06	0.16 ± 0.06	0.36 ± 0.06	0.14 ± 0.06
z^e	-0.03	0.003	$-0.9 \begin{cases} -0.5 \\ +0.3 \end{cases}$	$-3.1 \begin{cases} -2.4 \\ +1.0 \end{cases}$	$-1.4 \begin{cases} -0.5 \\ +0.4 \end{cases}$	$-6.6 \begin{cases} -5.8 \\ +2.2 \end{cases}$

^aSee Eq. (1).^bSee Eq. (2).^cThe experimental uncertainties are discussed in

Sec. III B.

^dSee Eq. (3).^eSee Eq. (4).

First of all, it is known that MR measurements have often been plagued with difficulties caused by the presence of impurities in the bulk, by contaminated sample surfaces, and by sample-end and probe effects. But here, as in the case of PbTe, the combination of high carrier density and high conductivity should make these problems unimportant. The high extrinsic positive carrier density, due to the Te excess, swamps out any effects from hard-to-remove impurities and surface contamination and the high conductivity minimizes current-distorting effects at the sample ends and at the points where the metallic probes contact the sample.

It is possible that the nonstoichiometry which produces the extrinsic carriers is not constant over the volume of a sample. The single crystals used for the MR measurements were selected from a large number of samples. Hall coefficient and Hall mobility data on these samples, which accumulated over a period of several years, but which were never published, are shown in Figs. 2 and 3. The results are smooth functions of p^* , except at $p_k^* \approx 2.5 \times 10^{20}$ cm⁻³, where a sharp kink in the Hall ratio R_{295}/R_0 appears and a slight droop in the μ_H data at 77 K may be detected. It is generally agreed that p_k^* is the nominal carrier density above which the low-temperature Fermi level drops below the subsidiary-valence-band maxima VB(Σ), so that holes appear in this region of the zone without the need for thermal excitation.^{38,39}

The data presented in Figs. 2 and 3 include all of the measurements made, not just those from selected crystals. The lack of scatter in the data

suggests that the samples were of uniform and reasonably high quality. However, it must be noted that this evidence is not as conclusive as it might be for crystals with more conventional characteristics. As Fig. 3 shows, the mobility is approximately proportional to $1/p^*$ at 295 and 77 K, so that the conductivity σ is only a weak function of p^* . This suggests that a nonuniform carrier density would not cause distorted current flow lines. In the usual case, current distortion would lead to an abnormally low σ .

On the other hand, current distortions should appear in a magnetic field, since the mobility and hence the Hall angle will be position dependent in an inhomogeneous sample. Unfortunately, any change in R , real or spurious, produces a self-compensating effect on μ_H ; i. e., the data point is moved along the true curve of μ_H vs p^* . However, the MR data ought to be sensitive to mobility inhomogeneities, producing a spurious effect which is proportional to the square of the mobility variation in the sample. Such an effect, if present, is evidently not very large in the SnTe MR data.

Furthermore, the Shubnikov-de Haas effect has been observed in many of the samples on which the measurements in Figs. 2 and 3 were made, including those used for the weak-field MR studies.^{39,43} As many as 60 oscillations were observed, implying that the carrier density over most of the volume of the sample is constant to within 1% or so.

We feel that the p^* range from which the SnTe MR measurements in Table I were obtained produced the highest possible data quality. At lower p^* ,

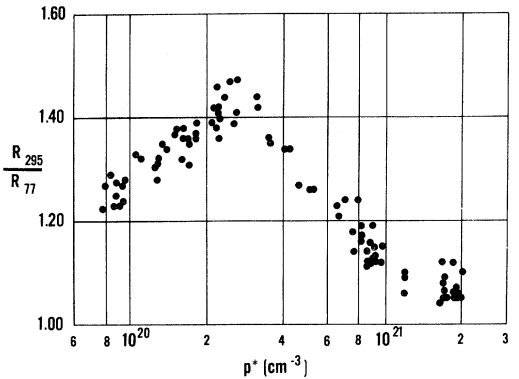


FIG. 2. Hall-coefficient ratio R_{295}/R_{77} vs nominal carrier density p^* for SnTe [$p^* = 1/(R_0 |e|)$; see Sec. III B].

very long anneal times (several months) were required to reach the composition limit of stability of the solidus field; inevitably, this raises some doubt that the limit was actually attained in the sample interior. On the other hand, since the weak-field MR varies as μ_H^2 and $\mu_H \propto 1/p^*$, the MR signals at higher p^* become much smaller and hence less accurate.

Partial sets of MR data taken on additional SnTe samples at or near the p^* values given in Table I, together with the limitations of the measuring apparatus, suggest that the SnTe MR coefficients are accurate to within ± 0.03 . If we assume that this accuracy is the variance in the errors of the MR coefficients and that these errors are normally distributed, the variances of the errors in $b, c,$ and d can be calculated. These variances are listed in Table I. An estimation of the accuracy of the MR symmetry parameter z presents a special problem in the case of SnTe because of the possibility of d being zero (see Sec. III A). In Table I we have listed the most probable values of z along with the largest changes in z which result from using all possible combinations of $b, c,$ and d within limits set by their variances. This analysis assumes that systematic errors are negligible. The justification for this assumption is the close fit of the corresponding PbTe data¹¹ (obtained under the same experimental conditions) to a model which has been verified by a number of independent experiments. The accuracy of the SnTe MR data is not as high as that obtained in the PbTe samples, but we ascribe most of this difference to the smaller size of the MR signals generated in SnTe.

C. Interpretive Problem

The behavior of weak-field MR has been useful in determining the orientation of the constant-energy surfaces in a number of multivalley semiconductors.⁸⁹

The simplest ellipsoid-of-revolution (EOR) multivalley models with over-all cubic symmetry predict the signs for $b + c$ and d and the specific values for the symmetry parameter z which are summarized in Table II.⁸⁹ It should be noted that the magnitudes of $b, c,$ and d are functions of the specific shape of the EOR, its orientation, the energy dependence of the scattering time, and the degree of degeneration of the statistics, while z depends only on the valley orientation. The coefficient d is a measure of the anisotropy of the constant-energy surfaces in the valleys. It reduces to zero for all of the models in Table II when the EOR becomes spherical, and its magnitude grows larger as they become more highly oblate or prolate.

The conditions under which the EOR results shown in Table II are valid will be discussed later in this section. Assuming for the moment that they are valid, a comparison with the experimental SnTe data in Table I suggests that the valleys are only slightly anisotropic, and that their orientations (if they are EOR) are not any of the three given in Table II. But these conclusions conflict with the evidence from the strong-field Shubnikov-de Haas and de Haas-van Alphen data which, as noted in Sec. I, suggest highly prolate $\langle 111 \rangle$ -oriented valleys.^{39,43,54}

An obvious generalization of these simple models is a combination of two sets of EOR. The main set would be $\langle 111 \rangle$ oriented and centered on the VB(L) maxima (as required by the known properties of the band structure of PbTe and SnTe listed in Sec. I). A second set of $\langle 110 \rangle$ or $\langle 100 \rangle$ EOR would be placed at appropriate points in the zone, at a

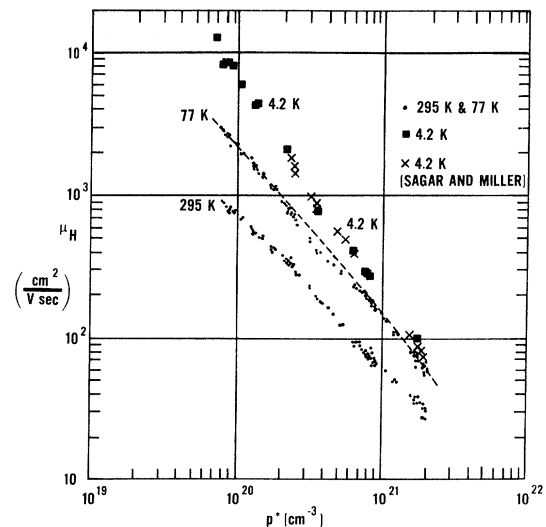


FIG. 3. Hall mobility μ_H vs nominal carrier density p^* for SnTe at 295, 77, and 4.2 K. Data of Sagar and Miller, Ref. 33, also included.

TABLE II. Magnetoresistance behavior in simple ellipsoid-of-revolution multivalley models.

Valley orientation	Sign of $b+c$	Sign of d	z
$\langle 111 \rangle$	0	+	0
$\langle 100 \rangle$	+	-	+1
$\langle 110 \rangle$	+	+	-1

slightly lower energy (i. e., of the order of kT lower). Then raising T would excite carriers from the first to the second set and cause z to deviate from zero. In this case, it does not matter whether the two sets of valleys belong to the same band or not.

This type of model is not suitable because the energy difference between the $VB(L)$ and $VB(\Sigma)$ maxima in SnTe is approximately 0.3 eV.^{40,46-49} Thus at the carrier densities in Table I, some deviation from $z=0$ might occur at room temperature but it would become negligible at 77 K. In contrast to this, Table I shows in fact that much larger deviations occur at the lower T .

We are forced then to return to a model which consists of a single set of valleys. Another simple way to explain symmetry values other than 0 and ± 1 is to consider ellipsoids of general shape, i. e., ellipsoids which are not surfaces of revolution.⁹⁰ An earlier attempt to explain the SnTe MR data used this approach.² The valley at each L point of the Brillouin zone was replaced by a cluster of ellipsoidal valleys on the hexagonal zone face on which the L point lies. The clusters were arranged so that the model retained over-all cubic symmetry. Two of the three principal axes of each valley were placed on the zone face, the third perpendicular to it.

This model was considered because it resembles the valence-band structure of Sb,⁹¹ the element which is isoelectronic to SnTe (see Sec. III F for a further discussion of the relevance of the Sb band structure). Fitting this model to the SnTe data at both carrier densities and temperatures, however, always led to ellipsoids which are very elongated in the plane of the zone face, i. e., *perpendicular* to the $\langle 111 \rangle$ directions. Since there are no other data to support such a model, and since it later came into direct conflict with the high-field data on SnTe, the model was not considered further.

Another attempt to account for the SnTe MR behavior^{41,56} used a prolate $\langle 111 \rangle$ -oriented surface-of-revolution version of the model developed by Morrell Cohen for Bi.⁹² The Cohen surface is non-ellipsoidal and nonparabolic, and its shape is a strong function of energy. The model does assume isotropic scattering; but one of the present authors has pointed out the equivalence of shape evolution and scattering anisotropy.⁹³ Hence the model is

quite a bit more general than the EOR or general ellipsoidal types, and would seem to be capable of reproducing the behavior of the MR symmetry parameter z . It is also a reasonable model, because of the Bi-SnTe familial connection.

The results of this calculation were surprising: It was found that z is restricted to the narrow interval between 0 and -0.3 , for wide ranges of the model parameters, including those which generate a highly distorted dumbbell-shaped Fermi surface. The only exception occurs when b , c , and d are all small. But this corresponds to a nearly spherical surface which is clearly not appropriate for SnTe. This unexpected result suggests that an explanation for the experimental data will require a model in which rotational invariance of the carrier properties about the $\langle 111 \rangle$ axes is *not* present.

Section IIID will consider the particular form that such a model might take. But first, we want to consider briefly a different approach to the problem of understanding the peculiar MR symmetry. Instead of making the Fermi-surface shape non-simple, we might generalize the nature of the carrier-scattering time on the surface, or even go so far as to say that it cannot be defined. The values $z=0$ and ± 1 given for the EOR models in Table II were obtained by making the standard assumptions that a scattering parameter may be substituted for the collision-integral part of the Boltzmann equation, and that the scattering time is isotropic or expressible as a diagonal tensor in the principal-axis coordinate system of each valley.

But this approach must be viewed in the light of the MR data for PbTe which are also summarized in Table I. In that case, the symmetry condition is precisely obeyed at two different temperatures, even though the scattering is not isotropic and even though the existence of a scattering time may be questioned. The first part of the above statement follows because the *mass* anisotropy is about 12 in p -type PbTe,^{31,94,95} while the *mobility* anisotropy lies between 4 and 5.^{11,30} The second part follows from the known importance of optical scattering,²⁶ for which a scattering time cannot always be defined.

The result $z=0$ for PbTe thus implies that the scattering time does exist and has the simple form which leads to that value. It seems unreasonable to make radically different assumptions about scattering in the closely related material SnTe.

Hence we return to the conclusion, based on both the high- and low-field MR data on SnTe, that the Fermi surfaces associated with the $VB(L)$ maxima are highly prolate and $\langle 111 \rangle$ oriented, but are not surfaces of revolution about these axes.

D. New Fermi-Surface Model

Recently, some new theoretical and experimental

information became available which suggested the next step. The theory was Cohen and Tsang's detailed calculation of the constant-energy surfaces in the VB(L) region of SnTe.⁷² They found that the cross sections perpendicular to the $\langle 111 \rangle$ symmetry axis of each valley change from circular to a distorted form with threefold rotational symmetry, as the plane of the cross section moves from the zone face into the interior of the zone. Ultimately, three knobs appear to be developing at each end of each valley.

On the experimental side, de Haas-van Alphen measurements on SnTe samples with $p^* = 6$ and $8 \times 10^{20} \text{ cm}^{-3}$ (which are greater than p_h^*) detected a new Fermi-surface cross section which is prolate and $\langle 100 \rangle$ oriented.⁵³ These pockets were discovered earlier, but their shape and orientation were not investigated.³⁹ Their $\langle 100 \rangle$ orientation, at first, seemed surprising, since the band-structure calculations suggested that the subsidiary-valence-band maxima were located along the $\langle 110 \rangle$ axes.

These results led us to develop the model shown in Fig. 4. It is presented in a stylized form which emphasizes the features needed to explain the weak-field MR data. It consists of a set of four highly distorted valleys centered on the VB(L) maxima and a second set of 12 prolate-ellipsoidal surfaces enclosing the subsidiary VB(Σ) maxima.

It is important to point out that Fig. 4, as drawn, implies that $p^* > p_h^*$ since the subsidiary pockets are shown occupied. The following explanation for the weak-field MR data (obtained at $p^* < p_h^*$) is based on the nature of the main VB(L) pockets alone. The subsidiary pockets were included in Fig. 4 in order to make it clear how $\langle 100 \rangle$ -oriented ellipsoids can appear along the $\langle 110 \rangle$ axes of the Brillouin zone. In addition, their presence focuses attention on the essential role played by the subsidiary VB(Σ) maxima: They are responsible for the sensitive manner

in which the shape of the main VB(L) pockets depends on p^* and T .

The arguments to support the appearance of the particular form of the distorted main VB(L) pockets shown in Fig. 4 are as follows: The inner ends of the eight half-ellipsoids of the $\langle 111 \rangle$ -EOR multi-valley model form the corners of a cube with edges which are parallel to the $\langle 100 \rangle$ directions of the Brillouin zone. These edges link each valley to its three nearest neighbors. The midpoints of the cube edges intersect the $\langle 110 \rangle$ axes of the zone near the VB(Σ) maxima. Because of these bridges of relatively high energy in the valence band, the main $\langle 111 \rangle$ -oriented valleys very rapidly deform as they increase in size, "reaching out" in the $\langle 100 \rangle$ directions towards their three nearest neighbors.

How will b , c , d , and z behave in such a model? One way to attempt to answer this question is by replacing each distorted Fermi surface in Fig. 4 by a combination of separate $\langle 111 \rangle$ - and $\langle 100 \rangle$ -oriented EOR of appropriate sizes. In a weak magnetic field, this will be a reasonable approximation to the true surface so long as the area in which the two models differ from each other constitutes only a small fraction of the total Fermi-surface area.

According to Table II, $b + c = 0$ and $d > 0$ for a $\langle 111 \rangle$ -EOR model, while $b + c > 0$, $d < 0$ for the $\langle 100 \rangle$ -EOR case. The initial effect of introducing a small fraction of $\langle 100 \rangle$ character into the purely $\langle 111 \rangle$ model will surely be to make $b + c > 0$, so that z will change from 0 to a negative value [see Eq. (4)]. As the $\langle 100 \rangle$ character increases in importance, d must decrease and ultimately change sign. As this is happening, $z \rightarrow -\infty$ and jumps to $+\infty$. A still stronger $\langle 100 \rangle$ character would cause z to approach $+1$.

In terms of this simple approximation to the true Fermi surface, the negative values of z found experimentally correspond to a combination of $\langle 111 \rangle$ and $\langle 100 \rangle$ symmetries, with the $\langle 111 \rangle$ character dominant. Thus the *small* positive d does not correspond to nearly spherical valleys but rather to the compensating effect of two types of symmetry which, separately, would produce *large* d values of opposite signs.

Since the $\langle 100 \rangle$ fingers will surely become more important as the carrier density grows, $-z$ should increase with increasing p^* . The dependence on T is less certain, because the relative motion of the VB(L) and VB(Σ) maxima in SnTe has not been definitely determined. But it seems more likely that E_v will decrease with decreasing T , as Fig. 1 suggests. This should cause the carriers to shift from the vicinity of VB(L) toward the VB(Σ) region; hence $-z$ should also increase with decreasing T . Both predictions are in accord with the trends in the z values summarized in Table I.

The result $d = 0$ for an as-grown crystal, men-

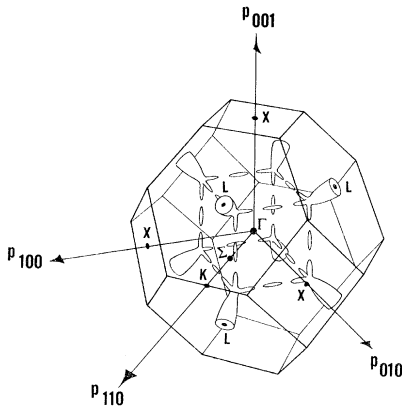


FIG. 4. Proposed Fermi-surface model for p -type SnTe. The form is exaggerated in order to bring out the main features clearly.

tioned in Sec. IIIA, may or may not be very accurate. If it is, however, it need no longer be regarded as a strange anomaly, but simply as the next event in the evolution of the distorted Fermi surface in Fig. 4, viz., the point at which the effects of the $\langle 100 \rangle$ and $\langle 111 \rangle$ anisotropies completely cancel.

The weak-field MR behavior for a combination $\langle 111 \rangle$ - and $\langle 100 \rangle$ -EOR multivalley model has already been calculated by Glicksman and applied to Ge-Si alloys.⁹⁶ For the present purposes, we examined the characteristics of the simplest possible version of such a model, namely one in which the two types of valleys have the same shape and the carriers in them have the same mobility. Then only one new variable is introduced, $f (= p_{100}/p_{111})$, the ratio of carrier density in one $\langle 100 \rangle$ to that in one $\langle 111 \rangle$ valley. We found that

$$z = -f / (\frac{1}{9} - f). \quad (5)$$

This result shows that relatively small knobs can have a major effect on the value of z , the obvious example being that $z \rightarrow -\infty$ as $f \rightarrow \frac{1}{9}$. In part, this is simply a consequence of the fact that there are six $\langle 100 \rangle$ knobs for each $\langle 111 \rangle$ valley.

It should be noted that a threefold distortion of a circular cross section is difficult to detect with high-field effects which measure Fermi-surface cross sections, because minimum and maximum radii occur opposite each other. Thus the angular variation in the *diameter* of the cross section is greatly diminished.

We have described the subsidiary VB(Σ) pockets as prolate ellipsoids merely because that is the simplest form consistent with the scanty experimental information about them.⁵⁴ It should be mentioned in passing that the appearance of the subsidiary pockets implies that the VB(Σ) points are relative maxima in the valence band. This is not a completely settled matter; they could be saddle points. In that case, no subsidiary pockets would appear at any p^* . Instead, the kinks in the Hall coefficient and mobility data (Figs. 2 and 3) at p_k^* would occur when the $\langle 100 \rangle$ knobs of the main valleys first touch each other on the $\langle 110 \rangle$ axes of the zone. This alternative would also lead to the appearance of a new cross section in the Shubnikov-de Haas or de Haas-van Alphen data. The trouble with this interpretation is that the carrier densities needed to bring the knobs together would seem to be much larger than the observed value of p_k^* .

E. Other Properties

Other puzzling results for SnTe which may now be understood in terms of the model in Fig. 4 are the elastic "constants" and the elastoresistance.

The elastic-stiffness-tensor components c_{44} and $c_{11} - c_{12}$, which correspond to two types of pure

shear, were both found to depend strongly on p^* in the range $(1.2-20) \times 10^{20} \text{ cm}^{-3}$.^{97,98} The magnitudes of the corresponding elastoresistance tensor components m_{44} and $\frac{1}{2}(m_{11} - m_{12})$ also turned out to be large for p^* between 1.8 and $19.6 \times 10^{20} \text{ cm}^{-3}$.⁵⁵

A general explanation for such characteristics was based on intervalley carrier transfer which occurs when the strain shifts the energy of some of the valleys relative to that of the remaining ones.⁹⁸ But only dc_{44}/dp^* and m_{44} are predicted to be large in a $\langle 111 \rangle$ -EOR model, and only $d(c_{11} - c_{12})/dp^*$ and $\frac{1}{2}(m_{11} - m_{12})$ in the $\langle 100 \rangle$ model, because in each case the other type of shear does not break the valley degeneracy.

The fact that the model proposed in this paper is a combination of $\langle 111 \rangle$ and $\langle 100 \rangle$ symmetries suggests how both types of shear can produce large effects in SnTe.

There have been a number of puzzling features of the behavior of the thermoelectric power, Hall coefficient, and Hall mobility in SnTe which have not been satisfactorily explained. We do not want to examine these features in detail in this paper, but we will point out in a general way how two characteristics of the model in Fig. 4 can be used to explain the experimental data.

The first characteristic is its very strong nonparabolicity. The Cohen and Dimmock models underestimate the nonparabolicity at higher carrier densities, because they do not take into account the important effects of the VB(Σ) maxima on the energy-momentum relationship as one moves away from the immediate vicinity of the VB(L) maxima. The second is the fact that the pockets which appear near VB(Σ) at $p^* > p_k^*$ do not constitute a second band. Therefore the properties of the carriers in the main and subsidiary pockets will become less and less different as the total carrier density increases and the two types of pockets approach each other.

The first feature makes it easier to understand how so many carriers are able to fit into what most analyses suggest is the rather small energy separation of the VB(L) and VB(Σ) maxima (but, as noted earlier, large compared to kT). It also makes the very small values of thermoelectric power observed for $p^* \leq p_k^*$, seem more reasonable. These values are depressed by the abnormally slow increase of σ with p^* .

Both features of the model help to explain the unusually rapid drop in μ_H with increasing p^* , the surprisingly small number of carriers in the subsidiary pockets for $p^* > p_k^*$,^{39,54} and the small perturbation of the mobility curve as p^* passes through p_k^* . The high effective-mass and low mobility values ascribed to the "second valence band" in some of the earlier analyses of SnTe transport data might just as well be associated with the high- p^* extrap-

ulations of the nonparabolic nature of the carriers in the main pockets.

Finally, there is the question of the Hall factor r , defined by the relation

$$R_0 = r/pe, \quad (6)$$

where p is the true carrier density. Consequently, using Eq. (1), $p = rp^*$. The kink in the Hall-ratio behavior shown in Fig. 2 suggests that a modest increase in r occurs for $p^* > p_k^*$. This is in accord with the two general properties of the proposed model cited above. However, the Hall data in Fig. 2 are not consistent with the results of direct measurements of r which indicate that $r = 0.6 \pm 10\%$ for p^* between 8.5×10^{19} and $2 \times 10^{21} \text{ cm}^{-3}$.³⁷

Tsu, Howard, and Esaki have argued that the two results can be reconciled, taking into account the experimental uncertainties.^{50,51} They calculated r using the Dimmock-Wright $\vec{k} \cdot \vec{p}$ model.⁵¹ As p^* increases, r decreases steadily for $p^* < p_k^*$, but this is counterbalanced by contributions from carriers in the subsidiary pockets when $p^* > p_k^*$.

Measurements of r at more closely spaced values of p^* are needed. The behavior of r vs p^* can have a crucial effect on the calculation of other properties such as the susceptibility effective mass in $\text{Pb}_{1-x}\text{Sn}_x\text{Te}$.^{57,83}

F. Comparisons with Band Structures of Bi, Sb, and Their Alloys

In this final discussion section, some similarities in the basic features of the band structures of the two alloy systems $\text{Pb}_{1-x}\text{Sn}_x\text{Te}$ and $\text{Bi}_{1-x}\text{Sb}_x$ will be identified.

First, we mention an earlier observation concerning the case $x=0$, i. e., PbTe and Bi . A very striking and direct connection between the band structures of these two materials was pointed out by Hall and Koenig.⁹⁹ The analogy they drew makes the now-accepted version of the band structure of Bi (about which so much controversy had swirled for many years) seem simple and obvious.

As noted in Sec. I, PbTe is a multivalley semiconductor with a direct gap at the four L points of the zone. If an extensive uniaxial stress is applied along one of the $\langle 111 \rangle$ directions, the lattice and the corresponding Brillouin zone acquire the trigonal symmetry found in Bi . The center of the hexagonal zone face normal to the stress axis is then called T , rather than L , as shown in Fig. 5.

Hall and Koenig noted that the experimentally determined piezoresistance coefficient for such a stress has opposite signs for extrinsic n - and p -type samples of PbTe . Those signs, plus the prolate nature of the energy surfaces near the conduction- and valence-band edges, establish that the energy at T rises relative to that at the three L points, in both bands.

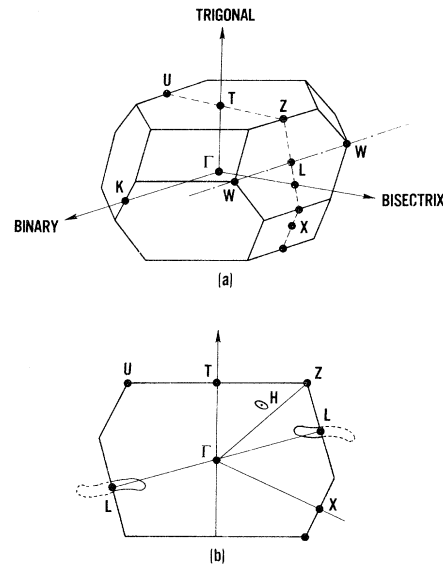


FIG. 5. (a) Brillouin zone for Sb. Dashed line identifies the vertical mirror plane $TL\Gamma$ and dash-dot line a twofold rotation axis WLW . (b) The mirror plane of (a), showing its intersection with a conduction-band valley (at L) and valence-band valley (at H). Not drawn to scale.

The stress, if it could be made large enough, would ultimately raise the valence-band energy at T above the conduction-band energy at the L points. In this simple direct way, the semimetallic Bi band structure—the three Shoenberg-tilted electron “ellipsoids” at the L points, plus the single hole EOR at T —is generated.

Here, we want to examine the case $x=1$, i. e., SnTe and Sb . In Sec. III C above, the calculation using the zone-face cluster model was described as an unsuccessful attempt to explain the SnTe MR data in terms of a Sb -like valence-band structure. It turns out after all that there are a number of strong links between the band structures of the two materials.

After years of confusion, it is now generally accepted that the Fermi surfaces in the conduction band of Sb (and As also) are qualitatively the same as those in Bi —three elongated surfaces at the L points, slightly tilted out of the plane which is perpendicular to the trigonal axis.¹⁰⁰

The shape of the constant-energy surfaces near the conduction-band minima is restricted by two symmetry operations at L , the vertical mirror plane ΓTL and the horizontal twofold rotation axis WLW which are identified in Fig. 5. Part (b) of this figure contains a sketch of the intersection of one of these Sb conduction-band valleys with the mirror plane through L . It has an S shape,¹⁰¹ curving away from the normal to the hexagonal-zone face at L , toward the T point on the adjacent

hexagonal face.

The first analogy to be noted for the case $x=1$ is that the corresponding mirror-plane cross section through an L point of the proposed SnTe model of Fig. 4 has the same kind of S-shaped cross section, due to the presence of the knobs. Presumably the distortion is present for the same reason in both SnTe and Sb—the surface is “reaching out” toward a neighboring region of the zone which lies in the same energy range.

There is a difference between the two cases: In Sb, there is only one mirror plane through a given L point, while in SnTe there are three (and three S-shaped cross sections), because in the latter case ΓL is an axis of threefold rotational symmetry. Despite this difference, however, there may well be two additional knobs near each end of the Sb conduction-band surface, lying on opposite sides of the mirror plane. We would not be surprised to learn that the corresponding bulges are also present in both the conduction- and valence-band surfaces of Bi. (As noted above, these distortions may be difficult to detect using the high-field techniques.)

One specific reason for giving up the original attempt to link the band structures of Sb and SnTe was that it became evident that the energy surfaces near the top of the valence band in SnTe enclose the L points (at least at the carrier densities studied) whereas the valence-band maxima in Sb have moved away from L (or T as it is called there) to a set of nearby points labelled H .⁹¹

One of the H points and the Fermi surface surrounding it are shown in Fig. 5. It lies on the reflection plane near the ΓZ lines which in the cubic zone would be the $\langle 110 \rangle$ axes ($\Gamma H = 0.52 \Gamma Z$; the angle between them is 11°). Furthermore, the Sb valence-band surfaces at H are elongated and point towards T ; i. e., they are approximately parallel to the ΓX directions which in the cubic case become the $\langle 100 \rangle$ axes.

Thus we find a second analogy at $x=1$: In location, shape, and orientation, the Fermi surfaces near the main maxima of the Sb valence band correspond very closely to the pockets associated with the subsidiary VB(Σ) maxima in the SnTe valence band. And these subsidiary maxima do have an important effect on the shape of the distorted constant-energy surfaces near the main VB(L) maxima of the SnTe valence band. In this sense then, the valence-band structures of SnTe and Sb are closely related.

In $\text{Bi}_{1-x}\text{Sb}_x$ alloys, Lerner, Cuff, and Williams¹⁰² and Golin¹⁰³ suggested that the levels which form the direct gap at the L points comes together and cross as Sb is added to Bi. This of course is directly analogous to the band-crossing model proposed by Dimmock, Melngailis, and Strauss for

the $\text{Pb}_{1-x}\text{Sn}_x\text{Te}$ alloys.⁷⁸

At the same time, however, the addition of Sb to Bi causes the valence-band energy maximum at T to decrease so rapidly that when $x=0.07 \pm 0.01$, it drops below the conduction-band minimum at L , and $\text{Bi}_{1-x}\text{Sb}_x$ becomes a semiconductor.

It seems likely that the addition of Sb to Bi *increases* the direct gap at T . It is therefore tempting to conclude that in Bi the conduction- and valence-band levels at T are the same as those at the L points, but in reversed order, i. e., they are already SnTe-like. The band-structure calculations do not bear this out. But since the levels involved are so close to each other and are so sensitive to details of the band calculation, this speculation should not be ruled out just yet.

IV. CONCLUSIONS

For a long time we had been puzzled by the peculiar behavior of the weak-field magnetoresistance in p -type SnTe, a behavior in very sharp contrast to that found in p -type PbTe. The acquisition of high-field Shubnikov-de Haas and de Haas-van Alphen data on SnTe did not improve the situation; in fact, it appeared that the low- and high-field data were not consistent.

In this paper we have described a Fermi-surface model which can resolve the apparent contradiction. The model was not specified analytically, but it was easy to describe in terms of its essential features, prolate $\langle 111 \rangle$ valleys to which are attached $\langle 100 \rangle$ -oriented knobs. We have tried to make the model more plausible by relating it to some general features of the band structures of the IV-VI compound semiconductors and the column-V semimetals.

We also examined in some detail a number of alternative approaches which could not account for the data. In so doing, we hope to have demonstrated the paramount importance of the symmetry axes of a multivalley model to the behavior of the weak-field magnetoresistance: Rotational invariance of carrier properties about specified axes tends to produce a characteristic weak-field symmetry, regardless of the detailed nature of the rotational invariance. But even modest deviations from that invariance can have a major effect on the weak-field MR symmetry.

We also noted that the kinds of distorted model discussed in this paper may be difficult to detect using the high-field oscillatory measurements. Cross sections of a Fermi surface perpendicular to its axis of threefold rotational symmetry may have a decidedly noncircular form, but the angular variation in the area of the set of cross sections in planes which include the symmetry axis are likely to be relatively small. We hope therefore to have shown that weak-field MR measurements

can sometimes be useful in the analysis of electronic properties outside of the band-edge region where they are normally used. Perhaps it can be worthwhile, under the appropriate circumstances, to attempt to interpret such data in an "intermediate" carrier density range extending from, say, 10^{19} to 10^{21} cm^{-3} .

ACKNOWLEDGMENTS

At long last, we would like to gratefully acknowledge the assistance of F. F. Bell, R. F. Bis, J. R. Burke, R. R. Clough, C. C. Evans, E. Gubner, M. K. Norr, P. O. Scheie, and D. J. Treacy in preparing the crystals and carrying out the transport measurements.

It is impractical to list all of those to whom we

are indebted for valuable discussions of the band structures of the IV-VI semiconductors and related materials, and the analysis of transport data. But the names that spring to mind immediately include H. J. Albany, A. A. Andreev, A. C. Beer, R. F. Brebrick, J. R. Burke, A. J. Crocker, M. L. Cohen, K. F. Cuff, J. R. Dixon, L. M. Falicov, R. F. Greene, J. F. Goff, W. E. Howard, V. I. Kaidanov, G. W. Pratt, S. Rabii, Yu. I. Ravich, H. R. Riedl, L. M. Rogers, A. Sagar, H. T. Savage, F. Stern, P. J. Stiles, A. J. Strauss, K. D. Tovstyuk, I. M. Tsidil'kovskii, R. Tsu, and J. Zemel. And finally we want to thank S. Dolan and G. Perkinson for their expert help in preparing the manuscript and figures.

[†]This work was supported by the Naval Ordnance Laboratory Independent Research Fund, by the Office of Naval Research (under Contract No. PO-9-0163), and by the Advanced Research Projects Agency (under order No. 1573).

¹R. S. Allgaier and B. B. Houston, *Bull. Am. Phys. Soc.* **7**, 331 (1962).

²R. S. Allgaier, C. C. Evans, and B. B. Houston, *Bull. Am. Phys. Soc.* **9**, 646 (1964).

³A preliminary report was presented earlier [R. S. Allgaier, *Bull. Am. Phys. Soc.* **15**, 304 (1970)]. It was also described in a discussion section on p. 317 of Ref. 6, but with an error: "(111)-directed knobs" should have been "(100)-directed knobs."

⁴IBM J. Res. Develop. **8**, 215-298 (1964).

⁵J. Phys. (Paris) **29**, C4-1-178 (1968).

⁶*The Physics of Semimetals and Narrow-Gap Semiconductors*, edited by D. L. Carter and R. T. Bate (Pergamon, Oxford, 1971).

⁷K. Shogenji and S. Uchiyama, *J. Phys. Soc. Japan* **12**, 1164 (1957).

⁸R. S. Allgaier, *Phys. Rev.* **112**, 828 (1958).

⁹W. W. Scanlon, *Solid State Phys.* **9**, 83 (1959).

¹⁰K. Shogenji, *J. Phys. Soc. Japan* **14**, 1360 (1959).

¹¹R. S. Allgaier, *Phys. Rev.* **119**, 554 (1960).

¹²R. S. Allgaier, *J. Appl. Phys.* **32**, 2185 (1961).

¹³R. S. Allgaier and B. B. Houston, in *Proceedings of International Conference on the Physics of Semiconductors*, edited by A. C. Stickland (The Institute of Physics and the Physical Society, London, 1962), p. 172.

¹⁴J. R. Dixon and H. R. Riedl, in Ref. 13, p. 179.

¹⁵K. F. Cuff, M. R. Ellett, and C. D. Kuglin, in Ref. 13, p. 316.

¹⁶H. R. Riedl, *Phys. Rev.* **127**, 162 (1962).

¹⁷J. R. Dixon and H. R. Riedl, *Phys. Letters* **12**, 164 (1964).

¹⁸J. R. Dixon and H. R. Riedl, *Phys. Rev.* **138**, A873 (1965).

¹⁹R. S. Allgaier and B. B. Houston, *J. Appl. Phys.* **37**, 302 (1966).

²⁰R. N. Tauber, A. A. Machonis, and I. B. Cadoff, *J. Appl. Phys.* **37**, 4855 (1966).

²¹A. A. Andreev and V. N. Radianov, *Fiz. Tekhn. Poluprov.* **1**, 183 (1967) [*Sov. Phys. Semicond.* **1**, 145 (1967)].

²²A. J. Crocker and L. M. Rogers, *Brit. J. Appl. Phys.* **18**, 563 (1967).

²³N. V. Kolomoets, M. N. Vinogradova, and L. M. Sysoeva, *Fiz. Tekhn. Poluprov.* **1**, 1222 (1967) [*Sov. Phys. Semicond.* **1**, 1020 (1968)].

²⁴L. M. Rogers, *Brit. J. Appl. Phys.* **18**, 1227 (1967).

²⁵A. A. Andreev, in Ref. 5, p. C4-50.

²⁶Yu. I. Ravich, B. A. Efimova, and I. A. Smirnov, *Semiconducting Lead Chalcogenides* (Plenum, New York, 1970).

²⁷A. A. Andreev, M. N. Vinogradova, B. A. Efimova, V. I. Kaidanov, N. V. Kolomoets, E. Ya. Lev, L. V. Prokof'eva, I. M. Rudnik, I. A. Smirnov, L. M. Sysoeva, and T. A. Chernik, in *Proceedings of the Ninth International Conference on the Physics of Semiconductors*, Moscow, 1968, edited by S. M. Rytvin and Yu. V. Shmartsev (Nauka, Leningrad, 1968), p. 1233.

²⁸I. A. Chernik, V. I. Kaidanov, M. N. Vinogradova, and N. V. Kolomoets, *Fiz. Tekhn. Poluprov.* **2**, 773 (1968) [*Sov. Phys. Semicond.* **2**, 645 (1968)].

²⁹W. Schilz, *J. Phys. Chem. Solids* **30**, 893 (1969).

³⁰O. S. Gryaznov and Yu. I. Ravich, *Fiz. Tekhn. Poluprov.* **3**, 1310 (1969) [*Sov. Phys. Semicond.* **3**, 1092 (1970)].

³¹J. R. Burke, B. B. Houston, and H. T. Savage, *Phys. Rev. B* **2**, 1977 (1970).

³²R. S. Allgaier and P. O. Scheie, *Bull. Am. Phys. Soc.* **6**, 436 (1961).

³³A. Sagar and R. C. Miller, in Ref. 13, p. 653.

³⁴R. F. Brebrick, *J. Phys. Chem. Solids* **24**, 27 (1963).

³⁵R. F. Brebrick and A. J. Strauss, *Phys. Rev.* **131**, 104 (1963).

³⁶J. A. Kafalas, R. F. Brebrick, and A. J. Strauss, *Appl. Phys. Letters* **4**, 93 (1964).

³⁷B. B. Houston, R. S. Allgaier, J. Babiskin, and P. G. Siebenmann, *Bull. Am. Phys. Soc.* **9**, 60 (1964).

³⁸B. B. Houston and R. S. Allgaier, *Bull. Am. Phys. Soc.* **9**, 293 (1964).

³⁹J. R. Burke, R. S. Allgaier, B. B. Houston, J. Babiskin, and P. G. Siebenmann, *Phys. Rev. Letters* **14**, 360 (1965).

⁴⁰B. A. Efimova, V. I. Kaidanov, B. Ya. Moizhes, and I. A. Chernik, *Fiz. Tverd. Tela* **7**, 2524 (1965) [*Sov. Phys. Solid State* **7**, 2032 (1966)].

⁴¹R. S. Allgaier, *Phys. Rev.* **152**, 808 (1966).

⁴²L. Esaki and P. J. Stiles, *Phys. Rev. Letters* **16**, 1108 (1966).

⁴³J. R. Burke, B. B. Houston, H. T. Savage, J.

- Babiskin, and P. G. Siebenmann, in *Physics of Semiconductors* (Physical Society of Japan, Tokyo, 1966), p. 384.
- ⁴⁴L. Esaki, in Ref. 43, p. 589.
- ⁴⁵P. J. Stiles, L. Esaki, and W. E. Howard, in *Proceedings of the Tenth International Conference on Low Temperature Physics*, edited by M. P. Malkov, M. Ya. Azbel', and V. S. Edelman (VINITI, Moscow, 1967), Vol. 3, p. 257.
- ⁴⁶A. A. Andreev, *Fiz. Tverd. Tela* **9**, 1560 (1967) [*Sov. Phys. Solid State* **9**, 1232 (1967)].
- ⁴⁷V. I. Kaidanov, I. A. Chernik, and B. A. Efimova, *Fiz. Tekhn. Poluprov.* **1**, 869 (1967) [*Sov. Phys. Semicond.* **1**, 723 (1967)].
- ⁴⁸H. Köhler, *Z. Angew. Phys.* **23**, 270 (1967).
- ⁴⁹L. M. Rogers, *J. Phys.* **1**, 845 (1968).
- ⁵⁰R. Tsu, W. E. Howard, and L. Esaki, *Phys. Rev.* **172**, 779 (1968).
- ⁵¹W. E. Howard, R. Tsu, P. J. Stiles, and L. Esaki, in Ref. 27, p. 93.
- ⁵²P. J. Stiles, in Ref. 5, p. C4-105.
- ⁵³J. R. Burke and H. R. Riedl, *Phys. Rev.* **184**, 830 (1969).
- ⁵⁴H. T. Savage and B. B. Houston, *Bull. Am. Phys. Soc.* **15**, 311 (1970).
- ⁵⁵A. Sagar, *J. Appl. Phys.* **41**, 811 (1970).
- ⁵⁶C. C. Evans, T. A. Reglein, and R. S. Allgaier, *Phys. Rev. B* **2**, 980 (1970).
- ⁵⁷R. F. Bis and J. R. Dixon, *Phys. Rev. B* **2**, 1004 (1970).
- ⁵⁸L. Kleinman and P. J. Lin, in *Physique des Semiconducteurs*, edited by M. Hulin (Dunod, Paris, 1964), p. 63.
- ⁵⁹G. W. Pratt and L. G. Ferreira, in Ref. 58, p. 69.
- ⁶⁰J. O. Dimmock and G. B. Wright, in Ref. 58, p. 77.
- ⁶¹J. O. Dimmock and G. B. Wright, *Phys. Rev.* **135**, A821 (1964).
- ⁶²J. B. Conklin, L. E. Johnson, and G. W. Pratt, *Phys. Rev.* **137**, A1282 (1965).
- ⁶³P. J. Lin and L. Kleinman, *Phys. Rev.* **142**, 478 (1966).
- ⁶⁴P. J. Lin, W. Saslov, and M. L. Cohen, *Solid State Commun.* **5**, 893 (1967).
- ⁶⁵M. L. Cohen, Y. Tung, and P. B. Allen, in Ref. 5, p. C4-163.
- ⁶⁶F. Herman, R. L. Kortum, I. B. Ortenburger, and J. P. van Dyke, in Ref. 5, p. C4-62.
- ⁶⁷S. Rabii, *Phys. Rev.* **182**, 821 (1969).
- ⁶⁸Y. W. Tung and M. L. Cohen, *Phys. Letters* **29A**, 236 (1969).
- ⁶⁹Y. W. Tung and M. L. Cohen, *Phys. Rev.* **180**, 823 (1969).
- ⁷⁰H. Overhof and U. Rössler, *Phys. Status Solidi* **37**, 691 (1970).
- ⁷¹R. L. Bernick and L. Kleinman, *Solid State Commun.* **8**, 569 (1970).
- ⁷²M. L. Cohen and Y. W. Tsang, in Ref. 6, p. 303.
- ⁷³J. O. Dimmock, in Ref. 6, p. 319.
- ⁷⁴Y. W. Tsang and M. L. Cohen, *Phys. Rev. B* **3**, 1254 (1971).
- ⁷⁵The first author is guilty of having fostered the use of this incorrect description. See Refs. 12 and 32.
- ⁷⁶B. A. Efimova, T. S. Stavitskaya, L. S. Stil'bans, and L. M. Sysoeva, *Fiz. Tverd. Tela* **1**, 1325 (1959) [*Sov. Phys. Solid State* **1**, 1217 (1960)].
- ⁷⁷B. A. Efimova and L. A. Kolomoets, *Fiz. Tverd. Tela* **7**, 424 (1965) [*Sov. Phys. Solid State* **7**, 339 (1965)].
- ⁷⁸J. O. Dimmock, I. Melngailis, and A. J. Strauss, *Phys. Rev. Letters* **16**, 1193 (1966).
- ⁷⁹J. R. Dixon and R. F. Bis, *Phys. Rev.* **176**, 942 (1968).
- ⁸⁰A. J. Strauss, *Trans. AIME* **242**, 354 (1968).
- ⁸¹J. W. Wagner and R. K. Willardson, *Trans. AIME* **245**, 461 (1969).
- ⁸²J. R. Burke, J. D. Jensen, and R. F. Greene, *Bull. Am. Phys. Soc.* **16**, 398 (1971).
- ⁸³Gaston Dionne, Ph.D. thesis (University of Ottawa, 1971) (unpublished).
- ⁸⁴J. Melngailis, T. C. Harman, J. G. Mavroides, and J. O. Dimmock, *Phys. Rev. B* **3**, 370 (1971).
- ⁸⁵J. W. Wagner, A. G. Thompson, and R. K. Willardson, *J. Appl. Phys.* **42**, 2515 (1971).
- ⁸⁶J. R. Burke, J. D. Jensen, and B. Houston, in Ref. 6, p. 393.
- ⁸⁷J. Melngailis, J. A. Kafalas, and T. C. Harman, in Ref. 6, p. 407.
- ⁸⁸B. B. Houston, R. F. Bis, and E. Gubner, *Bull. Am. Phys. Soc.* **6**, 436 (1961).
- ⁸⁹A. C. Beer, *Galvanomagnetic Effects in Semiconductors* (Academic, New York, 1963), Chap. 8.
- ⁹⁰R. S. Allgaier, *Phys. Rev.* **115**, 1185 (1959).
- ⁹¹L. M. Falicov and P. J. Lin, *Phys. Rev.* **141**, 562 (1966).
- ⁹²M. H. Cohen, *Phys. Rev.* **121**, 387 (1961).
- ⁹³R. S. Allgaier, *Phys. Rev. B* **2**, 3869 (1970); see also R. S. Allgaier, *Phys. Rev.* **165**, 775 (1968).
- ⁹⁴R. Nii, *J. Phys. Soc. Japan* **19**, 58 (1964).
- ⁹⁵H. Numata and Y. Uemura, *J. Phys. Soc. Japan* **19**, 2140 (1964).
- ⁹⁶M. Glicksman, *Phys. Rev.* **102**, 1496 (1956).
- ⁹⁷B. B. Houston and R. E. Strakna, *Bull. Am. Phys. Soc.* **9**, 646 (1964).
- ⁹⁸R. W. Keyes, *Solid State Phys.* **20**, 37 (1967).
- ⁹⁹J. J. Hall and S. H. Koenig, *Bull. Am. Phys. Soc.* **8**, 51 (1963).
- ¹⁰⁰G. A. Saunders, in Ref. 5, p. C4-3.
- ¹⁰¹J. B. Ketterson and L. R. Windmiller, *Phys. Rev. B* **1**, 463 (1970).
- ¹⁰²L. S. Lerner, K. F. Cuff, and L. R. Williams, *Rev. Mod. Phys.* **40**, 770 (1968).
- ¹⁰³S. Golin, *Phys. Rev.* **176**, 830 (1968).